Angewandte Chemie
Eine Zeitschrift der Gesellschaft Deutscher Chemiker

Supporting Information

Recovery of the Irreversible Crystallinity of Nanocellulose by Crystallite Fusion: A Strategy for Achieving Efficient Energy Transfers in Sustainable Biopolymer Skeletons**

Kazuho Daicho, Kayoko Kobayashi, Shuji Fujisawa, and Tsuguyuki Saito**

anie_202110032_sm_miscellaneous_information.pdf

SUPPORTING INFORMATION

Table of Contents

1. Experimental Procedures

Materials. A softwood dissolving pulp (Nippon Paper Industries, Japan) was used as the raw material. TEMPO, or 2,2,6,6-tetramethylpiperidine-1-oxyl, was purchased from Sigma-Aldrich, Japan. All other chemicals were purchased from FUJIFILM Wako Pure Chemical Corporation, Japan and were used as received.

CNF dispersion. The pulp (1 g) was TEMPO-oxidized with the addition of NaClO (5 mmol per gram of pulp) according to a previous report.[1] The oxidized pulp was then treated with $NaBH_4$ (0.1 g) in water (100 mL) at pH 10 for 3 h to eliminate unstable aldehyde groups. The carboxylate content of the oxidized pulp was determined to be ~1.3 mmol/g by conductivity titration. The hemicellulose content was ~3% (Xyl ~2%, Man ~1%) as determined by neutral sugar composition analysis. The oxidized pulp was suspended in water (0.1% w/w) and mechanically treated by using a Microtec Physcotron NS-56 homogenizer equipped with a 20-mm diameter shaft at 7500 rpm for 5 min, followed by sonication using a Nihon Seiki US-300T ultrasonic homogenizer equipped with a 26-mm diameter tip at 70% output for 6 min. The unfibrillated fraction in the suspension was removed by centrifugation at 12,000 g for 10 min, and the supernatant was collected as the CNF dispersion with sodium carboxylate groups.

CNF sheets. Sample *i* was prepared by freeze-drying of a 0.05% CNF dispersion containing 30% *tert*-butyl alcohol (80 mL),[2] followed by pressing at ~750 MPa for 1 min to be ~30 μm in thickness. Sample *ii* was prepared from a CNF dispersion concentrated to 0.4% at 40 °C using an rotary evaporator (80 mL), followed by evaporative drying in a 90-mm diameter polystyrene petri dish at 40 °C and 80% relative humidity for a week.[3] Sample *ii* was further immersed in a 0.1 M HCl solution for 2 h, followed by washing with distilled water and drying at 40 °C and 80% relative humidity to obtain sample *iii*. Sample *iii* was placed in a glass petri dish and subjected to hydrothermal treatment using a LSX-500 autoclave at 135 °C and 212 kPa for 30 min to prepare sample *iv*. Samples *i*–*iv* were all conditioned at 23 °C and 50% relative humidity before analysis. The moisture contents of samples *i*, *ii*, *iii* and *iv* were 5%, 8%, 5% and 4%, respectively.

TBA-bearing CNF. A 0.1 M HCl solution was add to a suspension of the oxidized pulp to adjust its pH to be ~2. After washing with distilled water, the pulp was suspended again in water, and a 10% TBA hydroxide solution was added to the suspension to adjust its pH to be ~8 according to a previously reported method;[4] here, the protonated carboxy groups in the pulp were neutralized with TBA hydroxide to form TBA carboxylate groups. The TBA-bearing CNF dispersion was obtained by wet disintegration of the pulp with TBA carboxylate groups as described above, and dried through the same process as adopted in the preparation of sample *ii*, followed by conditioning at 23 °C and 50% relative humidity before analysis.

HEC-covered CNF. A 0.2% w/w CNF dispersion with sodium carboxylate groups (72 g) was mixed with a 0.2% w/w HEC solution (8 g), followed by stirring for 1 day. The mixture was then dried through the same process as adopted in the preparation of sample *ii*, followed by conditioning at 23 °C and 50% relative humidity before analysis. The degree of substitution of HEC used was 1.6–1.8 according to the manufacture.

XRD. XRD measurements were performed in the reflection and transmission modes. In the reflection mode, the XRD profiles were obtained at diffraction angles 2θ ranging from 3–45° using a Rigaku Mini Flex diffractometer with Ni-filtered Cu Kα radiation (λ = 0.1542 nm) at 40 kV and 15 mA. The crystal size was calculated from the XRD peak corresponding to the (2 0 0) plane using Scherrer's equation (with a shape factor K = 0.9). Peak separation was performed according to a previous report.[6] In the transmission mode, the XRD diagrams was recorded on a Fujifilm imaging plate (2540 × 2540 pixels, 50 × 50 μm^2) at room temperature using a Rigaku MicroMax-007 HF system operating at 40 kV and 30 mA with Cu Kα radiation (λ = 0.15418 nm). The samples were set parallel to the X-ray beam, and the distance between the sample and imaging plate was calibrated using NaF. The recorded diagram was read using a Rigaku RAXIA-Di system and converted to a one-dimensional 2θ-intensity and azimuthal profiles using a Rigaku 2DP software. The degree of orientation (DO) was calculated from the azimuthal profile of the (2 0 0) reflection using the following equation.[7]

$$DO = \frac{180° - FWHM}{180°} \quad (1)$$

where FWHM is the full width at half maximum.

SUPPORTING INFORMATION

CP/MAS ^{13}C NMR spectroscopy. CP/MAS ^{13}C NMR measurements were performed using a JEOL JNM-ECAII 500 spectrometer (JEOL Ltd., Tokyo, Japan) equipped with a 3.2-mm HXMAS probe and ZrO_2 rotors at 125.77 MHz for ^{13}C. The samples were spun at 15000 Hz and the 90° proton decoupler pulse width, contact time, and relaxation delay were set to 2.5 μs, 2 ms, and 5 s, respectively.[5] Adamantane was used as the internal standard for the ^{13}C chemical shifts. The C4 and C6 crystallinity indices were calculated as the area ratio of the crystalline and noncrystalline signals in the C4 and C6 regions, respectively. Peak separation was performed according to the method described in a previous report.[6]

XRD simulation. The single CNF model consisting of 18 cellulose chains was constructed using a Visualizer module in the BIOVIA Material Studio 2020 software, based on the atomic coordinates of the crystal unit of cellulose Iβ crystallite, reported by Nishiyama *et al.*.[10] In the 18-chain model, the cellulose molecular sheets were stacked in 2/3/4/4/3/2 chain modes with crystal sizes of the (110), (1-10), and (200) planes of 3.10 nm, 2.12 nm, and 2.34 nm, respectively.[7] The model was extended by two cellobiose units along the *c* axis, according to a previous report.[8] The 23 types of model where two CNFs assembled were constructed as shown in Figures 3 and S7. The XRD patterns of these models were simulated using a Forcite module in the software based on Debye's scattering formula:

$$I(Q) = \sum_{\mathrm{i}} \sum_{\mathrm{j}} f_{\mathrm{i}} f_{\mathrm{j}} \frac{\sin\left(Q r_{\mathrm{ij}}\right)}{Q r_{\mathrm{ij}}} \tag{2}$$

where Q is the scattering vector, described as $Q = |Q| = 4\pi \sin\theta / \lambda$ (θ: the diffraction half-angle, λ: wavelength), f_{i} and f_{j} are the atomic scattering factors of the radiation used, and r_{ij} denotes the vector connecting atoms *i* and *j*. The X-ray and cut-off wavelengths for the calculation were set to 1.54178 and 40 Å, respectively. For comparing the simulated XRD patterns with the experimental pattern, the correlation coefficient, R^2, was calculated using the following equation:

$$R^2 = \frac{\sum (x - x')(y - y')}{\sqrt{\sum (x - x')^2 (y - y')^2}} \tag{3}$$

where *x* and *y* are the relative intensities of the simulated and experimental XRD in the range of 2θ = 12–32°, respectively; and *x′* and *y′* are average intensities of the simulated and experimental XRD, respectively.

Thermal properties. The thermal diffusivity, *α*, values in the out-of-plane direction were measured at 10 different locations for each sample using thermal wave analysis with an ai-Phase Mobile 1u at 23 °C and 50% relative humidity. The applied voltage was 0.8 V, and the delay in the phase of the temperature wave (with an amplitude of ± 0.5 °C) was measured at 10 points within a range of 6−60 Hz for each sheet pot. The integration time for each point was typically 10 s. During the measurement, the entire device was covered with an optically opaque windshield. The thermal conductivity, *k*, was calculated from *α* using the following equation:

$$k = \alpha c \rho \tag{4}$$

where *c* is the specific heat capacity, and *ρ* is the bulk density. The specific heat capacity *c* was measured using a Perkin Elmer DSC8500 instrument in the temperature range of 0−40 °C at a heating rate of 10 °C/min.

Other analyses. The porosities of the samples were calculated using the following equation:

$$porosity = 1 - \frac{Bulk\ density \times (1 - Moisture\ content)}{true\ density} \tag{5}$$

The true densities were measured using a BELPycno helium pycnometer according to a previously reported method.[9] The bulk densities were calculated from their volumes and weights at 23 °C and 50% relative humidity. The moisture contents were calculated from the sample weights at 23 °C and 50% relative humidity and those after drying at 105 °C for 3 h. The scanning electron microscopy (SEM) images were captured with a Hitachi S-4800 field-emission microscope at 1 kV. The samples for SEM were pretreated with a Meiwafosis Neo osmium coater at 5 mA for 10 s. The nitrogen adsorption–desorption isotherm was measured with a Quantachrome NOVA 4200e at −196 °C after degassing the samples in the system at 105 °C for 3 h. The SSA values of the samples were estimated from the isotherms according to Brunauer-Emmett-Teller theory. The sample weights were measured after degassing.

2. Supplementary Figures

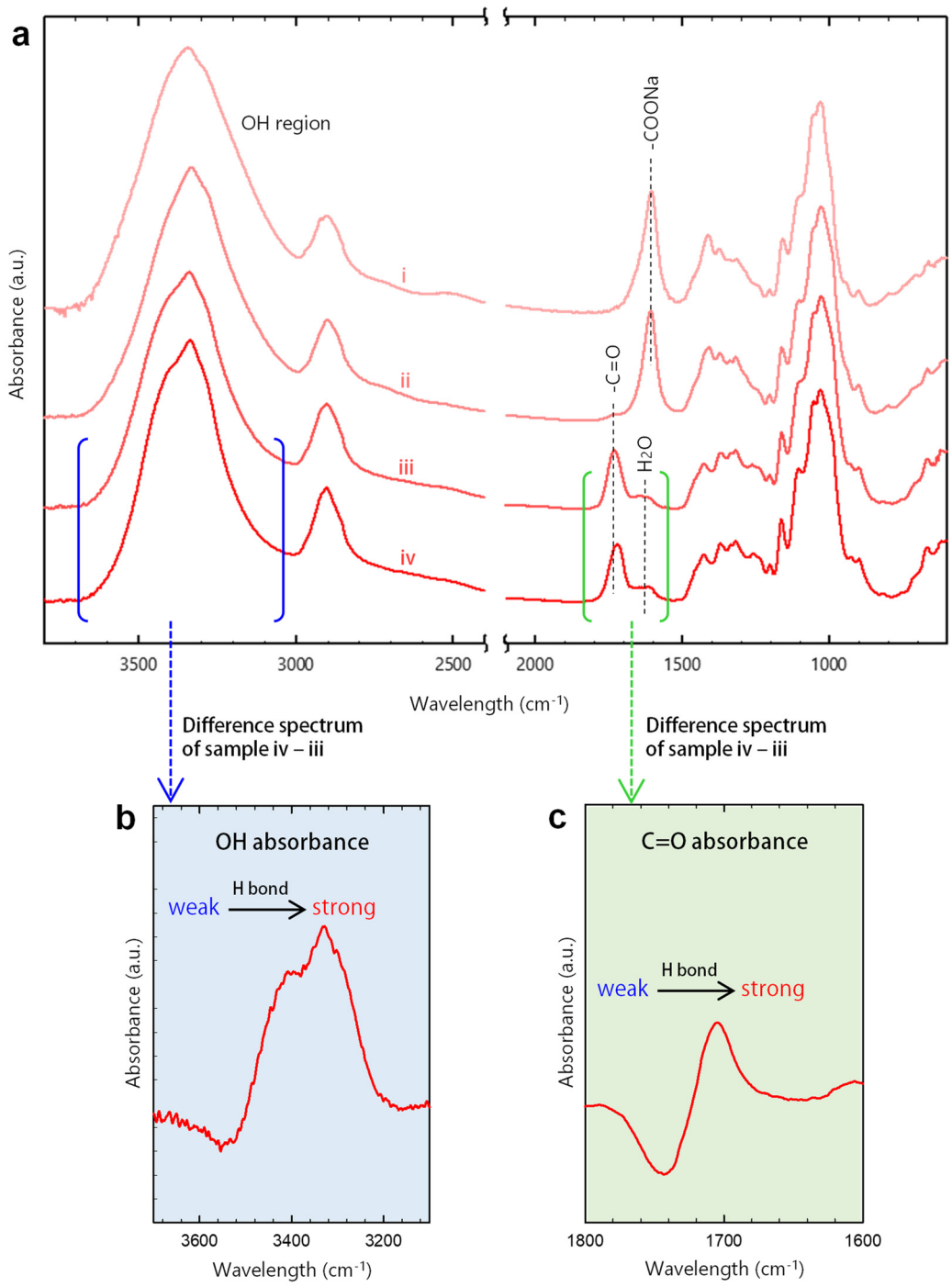

Figure S1. (a) FTIR spectra of samples *i*–*iv*, and (b, c) the deference spectra obtained by subtracting the FTIR spectrum of sample *iii* from that of sample *iv* in the (b) OH and (c) C=O regions. The absorption at ~1720 cm^{-1} is assigned to the C=O stretching of the surface carboxy groups forming hydrogen bonds,[10] and the red shifting in the deference spectra shows that the hydrogen bonds in sample *iv* were stronger than those in sample *iii*.

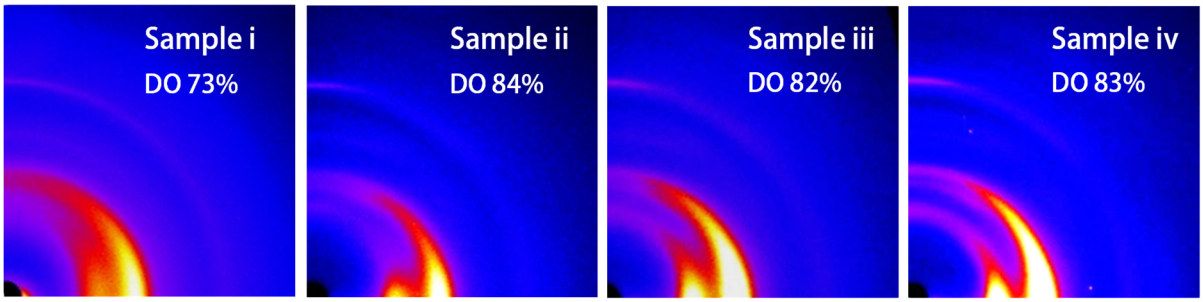

Figure S2. XRD diagrams of samples i–iv set parallel to the beam. The DO values, which were calculated from the diagrams, show the degree of orientation of the CNFs in each sheet-like sample to the sheet plane.

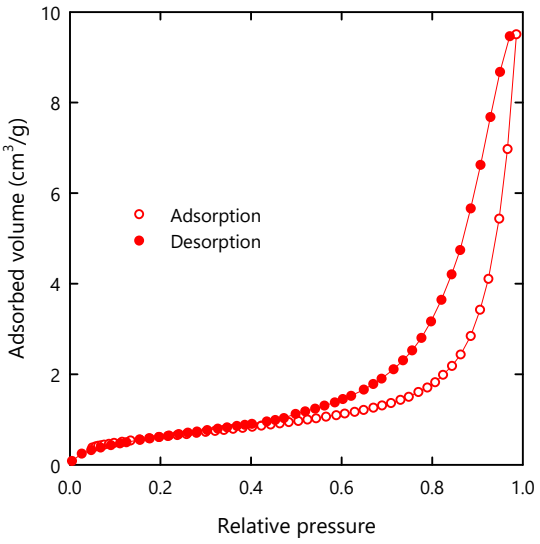

Figure S3. Nitrogen adsorption–desorption isotherm of sample *i*.

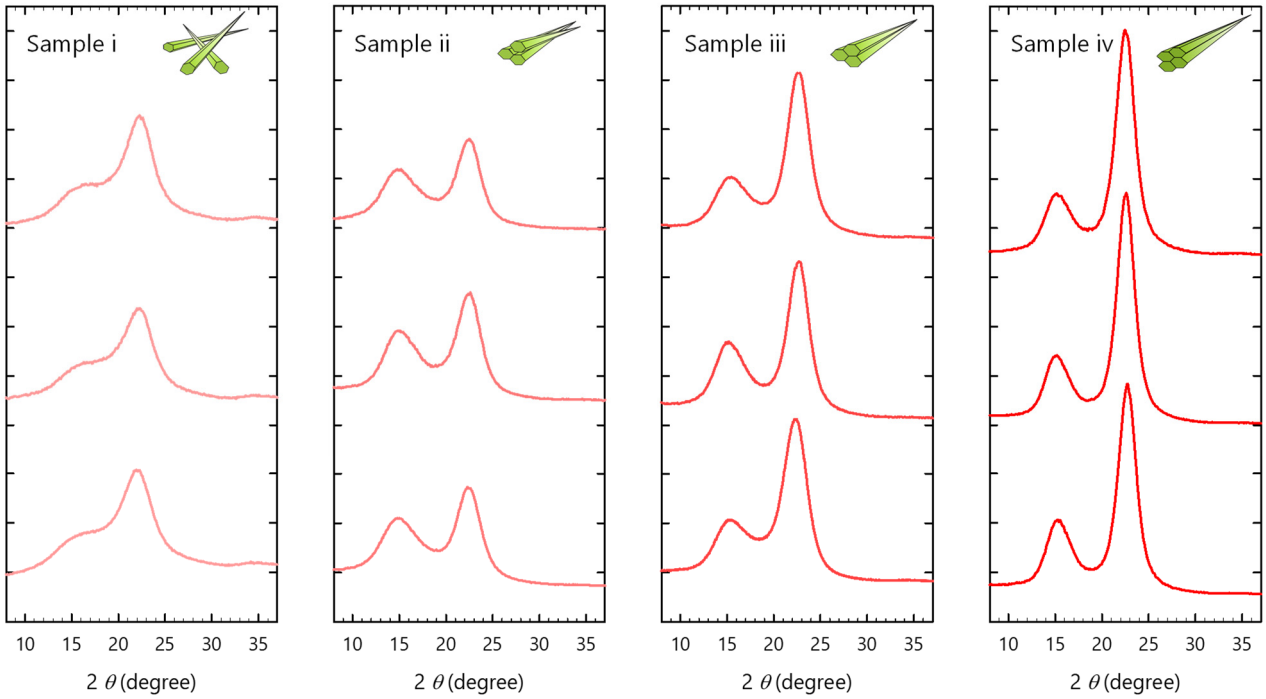

Figure S4. XRD profiles of three set of samples *i–iv* prepared from a CNF dispersion with carboxylate and hemicellulose contents of ~1.3 mmol/g and 3%, respectively. The raw material of the dispersion was a softwood dissolving pulp (see Experimental section).

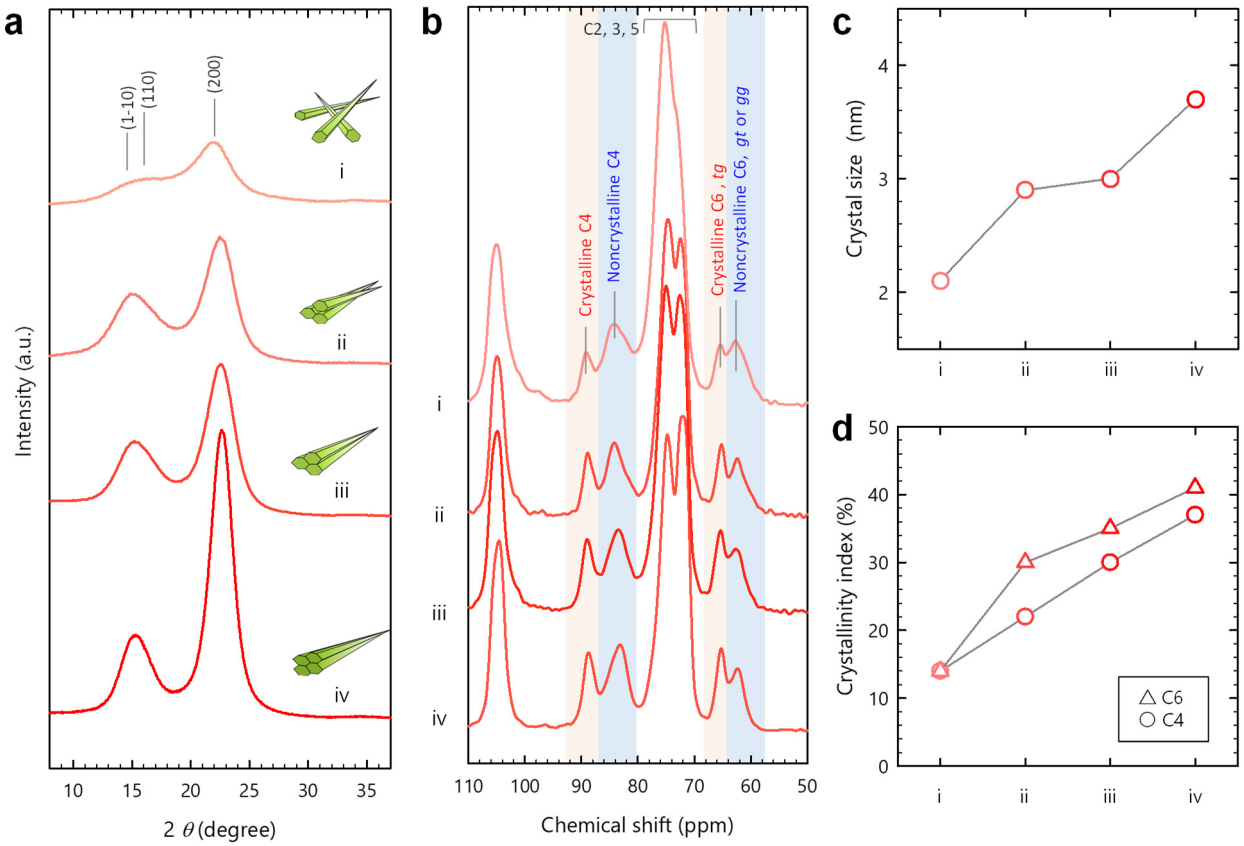

Figure S5. (a) XRD profiles and (b) CP/MAS ^{13}C NMR spectra of samples *i–iv* prepared from another CNF dispersion with carboxylate and hemicellulose contents of ~1.3 mmol/g and 6%, respectively. A softwood bleached kraft pulp was used as the raw material. (c) Crystal size of the (2 0 0) plane calculated from the XRD profiles, and (d) crystallinity indices of the C4 and C6 carbon atoms calculated from the NMR spectra.

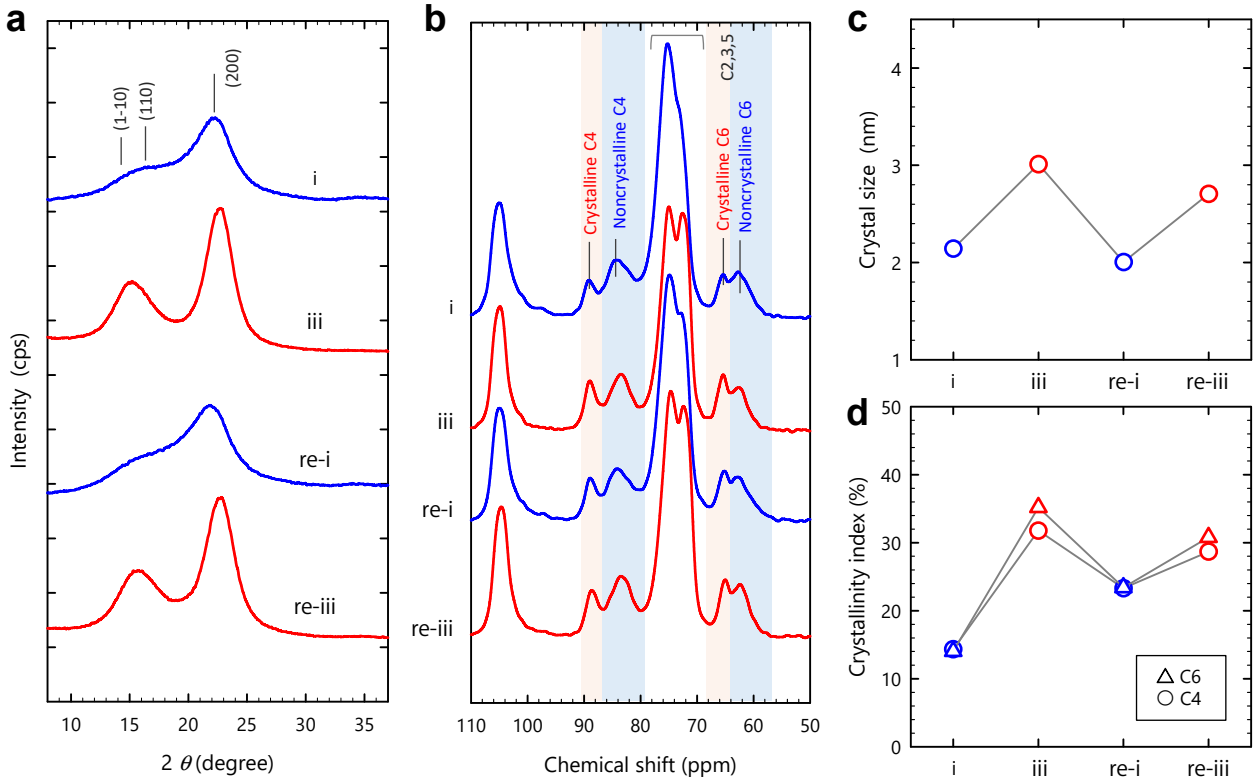

Figure S6. Repeatability of the crystallinity recovery. Sample *iii* was disintegrated into CNFs in water, and dried again through the same freeze-drying process as adopted in the preparation of sample *i*; thus, it is coded here as reproduced sample *i*, re-*i*. The sample re-*i* was then swelled in water and dried again through the same process as adopted in the preparation of samples *iii*; thus, it is coded here as reproduced sample *iii*, re-*iii*. (a) XRD profiles and (b) CP/MAS ^{13}C NMR spectra of samples *i*, *iii*, re-*i*, and re-*iii*. c) Crystal sizes of the (2 0 0) plane calculated from the XRD profiles. (d) Crystallinity indices of the C4 and C6 carbon atoms calculated from the NMR spectra.

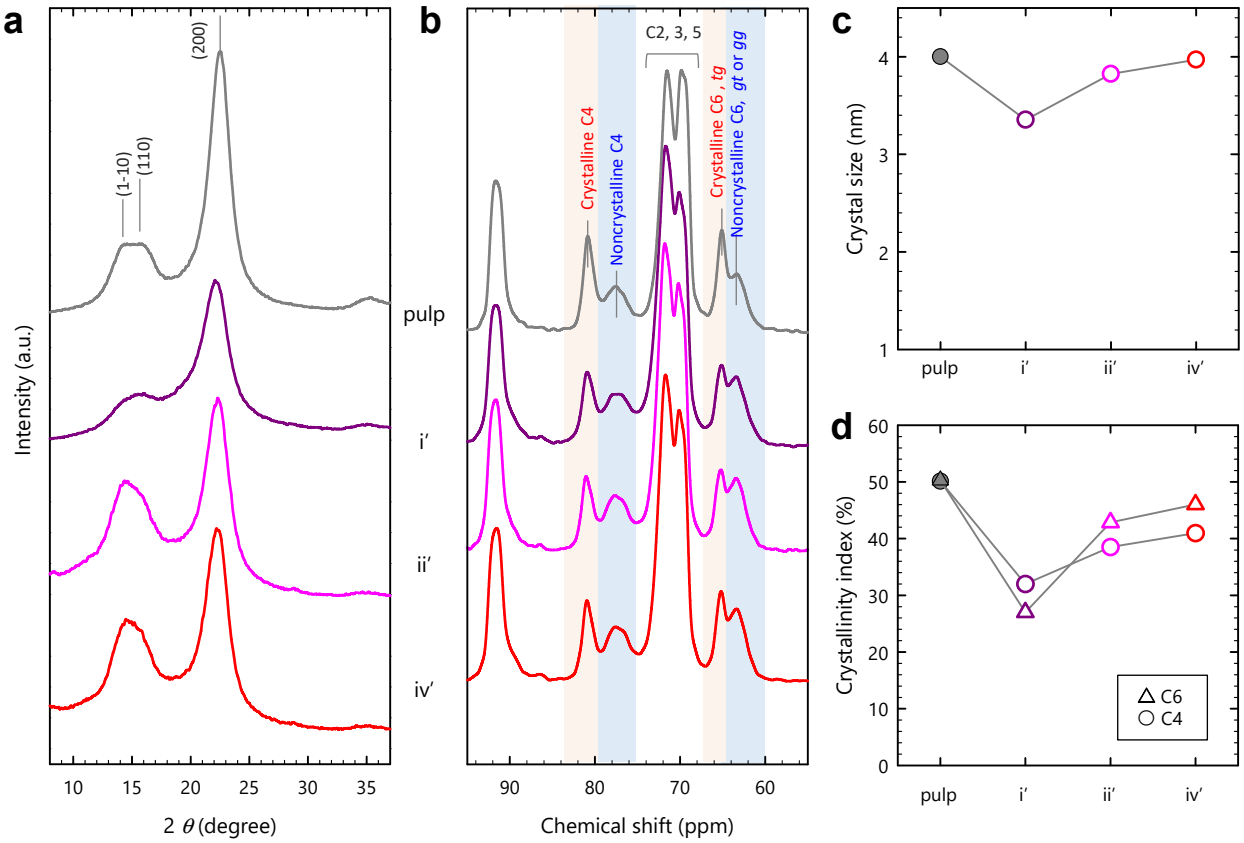

Figure S7. Crystallinity recovery of chemically unmodified CNFs. The CNFs were produced from the dissolving pulp solely by wet disintegration. These CNFs were assembled through the same process as adopted in the preparation of sample *i*, *ii*, or *iv*; thus, they are coded here as samples *i*′, *ii*′, and *iv*′, respectively. (a) XRD profiles and (b) CP/MAS ^{13}C NMR spectra of the pulp and samples *i*′, *ii*′, and *iv*′. (c) Crystal sizes of the (2 0 0) plane calculated from the XRD profiles. (d) Crystallinity indices of the C4 and C6 carbon atoms calculated from the NMR spectra.

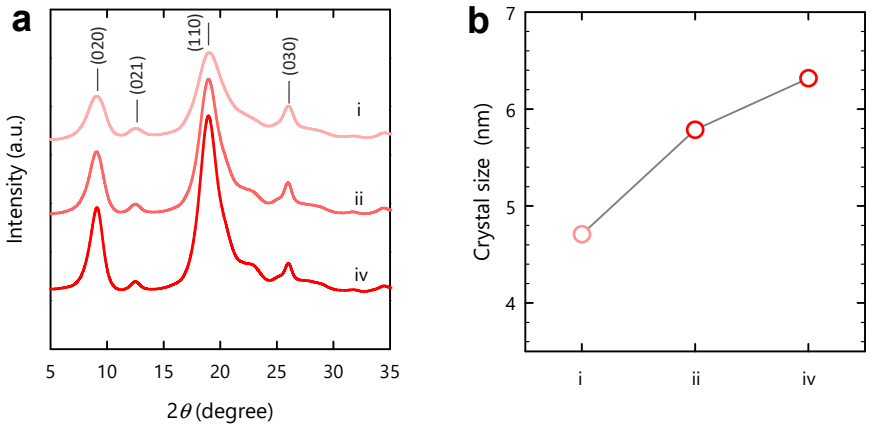

Figure S8. Crystallinity recovery of α-chitin fibrils. The chitin fibrils were dispersed in water according to a previous report,[11] and were then assembled through the same drying process as adopted in the preparation of samples *i*, *ii*, and *iv*; thus, they are coded here as chitin *i*, *ii*, and *iv*, respectively. (a) XRD profiles of chitin *i*, *ii*, and *iv*. (b) Crystal sizes of the (0 2 0) plane calculated from the XRD profiles.

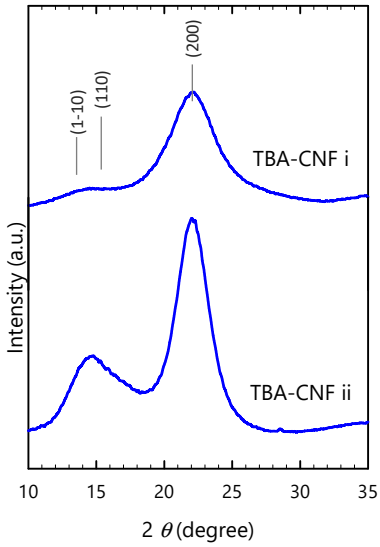

Figure S9. XRD profiles of TBA-CNF *i* and *ii* prepared from a TBA-CNF dispersion through the same drying process as adopted in the preparation of samples *i* and *ii*, respectively. The data for the TBA-CNF in Figure 2 were collected from the TBA-CNF *ii* here.

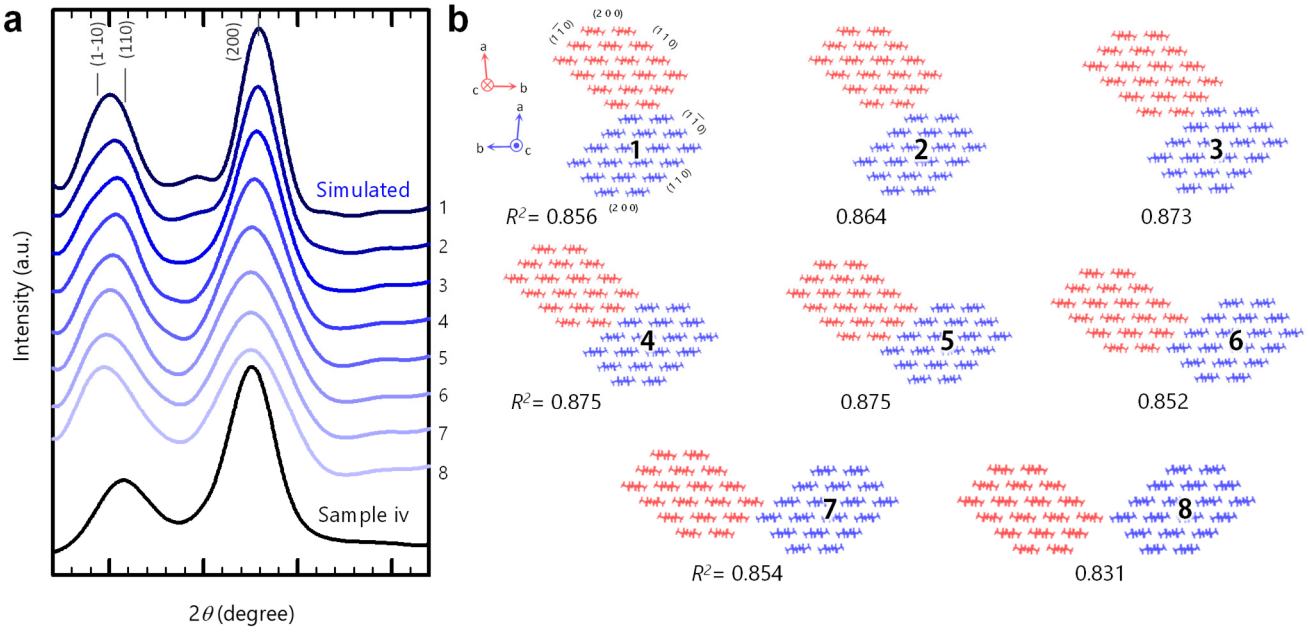

Figure S10. (a) Comparison of the XRD profile of sample *iv* with the simulated profiles of (b) the antiparallel CNF models #1–8.

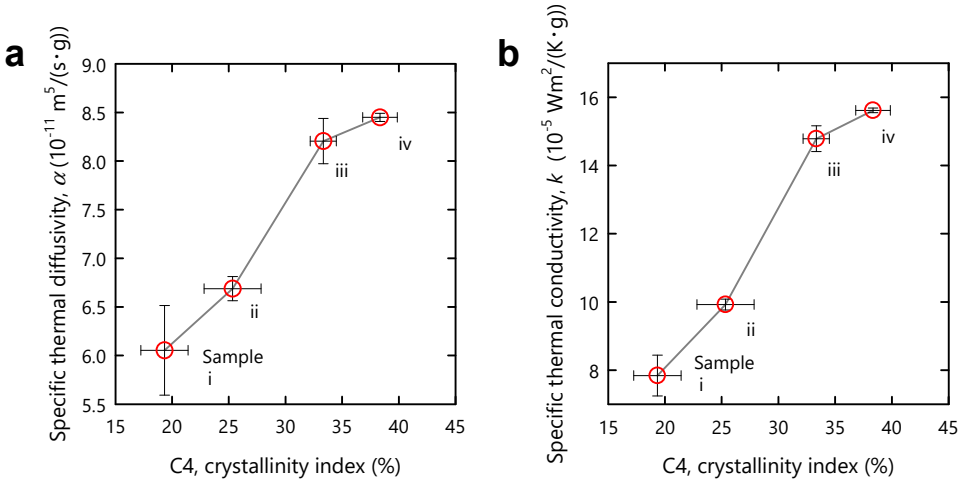

Figure S11. (a) Thermal diffusivities, *α*', and (b) conductivities, *k*', divided by their bulk densities for samples *i–iv* as a function of the crystallinity index of the C4 carbon atoms.

3. References

[1] T. Saito, Y. Nishiyama, J. Putaux, M. Vignon, A. Isogai, *Biomacromolecules* **2006**, 7, 1687-1691.
[2] J. Nemoto, T. Saito, A. Isogai, *ACS Appl. Mater. Interfaces* **2015**, 7, 19809-19815.
[3] M. Zhao, F. Ansari, M. Takeuchi, M. Shimizu, T. Saito, L. Berglund, A. Isogai, *Nanoscale Horiz.* **2018**, 3, 28-34.
[4] M. Shimizu, T. Saito, A. Isogai, *J. Membr. Sci.* **2016**, 500, 1-7.
[5] K. Daicho, S. Fujisawa, K. Kobayashi, T. Saito, J. Ashida, *J. Wood Sci.* **2020**, 66, 62.
[6] K. Daicho, T. Saito, S. Fujisawa, A. Isogai, *ACS Appl. Nano Mater.* **2018**, 1, 5774-5785.
[7] Y. Nishiyama, P. Langan, H. Chanzy, *J. Am. Chem. Soc.* **2002**, 124, 9074-9082.
[8] J. D. Kubicki, H. Yang, D. Sawada, H. O'Neill, D. Oehme, D. Cosgrove, *Scientific Reports* **2018**, 8, 1-8.
[9] K. Daicho, K. Kobayashi, S. Fujisawa, T. Saito, *Biomacromolecules* **2020**, 21, 3, 939-945.
[10] S. Fujisawa, Y. Okita, H. Fukuzumi, T. Saito, A. Isogai, *Carbohydrate Polymers* **2011**, 84, 579-583.
[11] Y. Kaku, S. Fujisawa, T. Saito, A. Isogai, *Biomacromolecules* **2020**, 21, 1886-1891.